Journal of Cellular and Molecular Medicine
A JOURNAL OF TRANSLATIONAL MEDICINE

J. Cell. Mol. Med. Vol 15, No 11, 2011 pp. 2364-2376

Regulation of dynamin-2 assembly–disassembly and function through the SH3A domain of intersectin-1s

Ivana Knezevic [a], Dan Predescu [a], Cristina Bardita [a], Minhua Wang [a], Tiffany Sharma [b], Barbara Keith [b, †], Radu Neamu [c], Asrar B. Malik [b], Sanda Predescu [a, *]

[a] *Department of Pharmacology, Rush University Medical Center, Medical College, Vascular Biology Section, Chicago, IL, USA*
[b] *Department of Pharmacology, University of Illinois at Chicago, College of Medicine, Chicago, IL, USA*
[c] *Saint Raphael Hospital, New Haven, CT, USA*

Received: July 12, 2010; Accepted: November 18, 2010

Abstract

Intersectin-1s (ITSN-1s), a five Src homology 3 (SH3) domain-containing protein, is critically required for caveolae and clathrin-mediated endocytosis (CME), due to its interactions with dynamin (dyn). Of the five SH3A-E domains, SH3A is unique because of its high affinity for dyn and potent inhibition of CME. However, the molecular mechanism by which SH3A integrates in the overall function of ITSN-1s to regulate the endocytic process is not understood. Using biochemical and functional approaches as well as high-resolution electron microscopy, we show that SH3A exogenously expressed in human lung endothelial cells caused abnormal endocytic structures, distorted caveolae clusters, frequent staining-dense rings around the caveolar necks and 60% inhibition of caveolae internalization. *In vitro* studies further revealed that SH3A, similar to full-length ITSN-1s stimulates dyn2 oligomerization and guanosine triphosphatase (GTP)ase activity, effects not detected when other SH3 domains of ITSN-1s were used as controls. Strikingly, in the presence of SH3A, dyn2–dyn2 interactions are stabilized and despite continuous GTP hydrolysis, dyn2 oligomers cannot disassemble. SH3A may hold up caveolae release from the plasma membrane and formation of free-transport vesicles, by prolonging the lifetime of assembled dyn2. Altogether, our results indicate that ITSN-1s, *via* its SH3A has the unique ability to regulate dyn2 assembly–disassembly and function during endocytosis.

Keywords: intersectin-1s • dynamin-2 • caveolae • endocytosis • SH3 domains • endothelium

Introduction

Caveolae[1] are vesicular carriers that function in endocytosis and transcytosis in different cell types such as endothelial cells (ECs) [1, 2], epithelial cells [3], osteoclasts [4] and neurons [5]. Endothelial transcytosis *via* caveolae is the most studied and best documented system of transcellular transport [6]. During transcytosis, caveolae shuttle between the two fronts of the cell, undergoing fusion–fission events at each round of transport [7]. Caveolae are equipped with a full set of fusion and fission proteins organized in supramolecular protein lipid-complexes, containing soluble N-ethylmaleimide sensitive factor attachment proteins (SNAPs) and SNAP receptors (SNAREs), dynamin (dyn)2, regulatory proteins and lipids [8]. The presence of dyn2 in the endothelial fusion–fission complexes is a requirement for a process that couples rapidly and efficiently endocytosis to exocytosis on opposite sides of the plasma membrane (PM). Studies on caveolae internalization have demonstrated that caveolae release from the PM and formation of free transport vesicles is dyn2 and intersectin-1s (ITSN-1s) dependent [9, 10]. Electron microscopy (EM) immunogold labelling indicated that both, dyn2 and ITSN-1 are concentrated on caveolae and associate preferentially with the neck region of caveolae [10]. ITSN-1s, a widely

[†]Present Address: Montana State University, Bozeman, MT 59717, USA.
*Correspondence to: Sanda PREDESCU, Ph.D.,
Department of Pharmacology, Rush University Medical Center,
Medical College, Vascular Biology Section, 1735 W Harrison,
Chicago, IL 60612, USA.
Tel.: 312–563-2437
Fax: 312–942-0339
E-mail: sanda_predescu@rush.edu

[1]Since in endothelial cells the true caveolae (vesicular carriers caveolin-1$^+$) represent ~95% of the whole vesicular population and since, the non-caveolin-1 and non-clathrin vesicles identified in the caveolin-1 null mouse are poorly represented and not yet well defined as a caveolin-1- and clathrin-independent vesicular transport system [6], we will use the term caveolae as being synonymous with all non-clathrin vesicular carriers.

doi: 10.1111/j.1582-4934.2010.01226.x

expressed and highly conserved protein, comprises several protein-iprotein interaction modules, including two NH_2-terminus Eps15 homology domains, a central coiled-coil domain and five consecutive Src Homology 3 (SH3A-E) domains [11, 12]. Studies have shown that ITSN-1s plays important roles in endocytosis [10, 13, 14], MAPK signalling [15], cell survival and apoptosis [16, 17]. The involvement of ITSN-1s in endocytosis was first revealed when a Xenopus Laevis oocyte cDNA expression library screened with a SH3 class II peptide ligand revealed a protein that binds two endocytic proteins, dyn1 and synaptojanin [11]. Later on, ITSN-1 was implicated in endocytosis based on interactions with other endocytic proteins, including epsins [18], secretory carrier membrane protein (SCAMP)-1 [12, 19], mSos [20] and neuronal Wiscott-Aldrich syndrome protein (N-WASP) [21, 22]. Overexpression of full-length ITSN-1s or SH3A-E domains alone specifically inhibits caveolae and clathrin-mediated endocytosis (CME) [10, 11, 23]. Specific silencing of ITSN-1 gene in ECs caused significant decrease in caveolae number and triggered the mitochondrial cell death, suggesting a complex role of this protein in ECs survival [16]. Furthermore, stable silencing of ITSN expression increased apoptosis in both neuroblastoma and primary cortical neurons, by interfering with PI3K-C2β-protein kinase B (AKT) survival pathway [17]. Substantial interest has been focused on the interaction of ITSN-1, *via* the SH3 domains, with the proline-rich domain (PRD) of dyn. Among ITSN's SH3 domains, the SH3A displays the highest affinity for dyn [11], and is one of the most potent inhibitor of CME [23]. Overexpression of a truncated ITSN-1s lacking the SH3A causes significant inhibition of caveolae trafficking [10], most likely by non-productive dyn2 recruitment to the caveolae endocytic site. Recently, the role of ITSN-1 as a general endocytic protein has been confirmed by studies of ITSN-1 null mice which display alteration of endocytic and vesicle trafficking events, in both neuronal and non-neuronal cells [24]. However, despite an increasing body of evidence suggesting that the SH3 domain containing proteins interfere with endocytosis in the dyn-controlled scission step, at present the molecular mechanisms of this blockage is not well understood. Dyn2, the ubiquitously expressed isoform of the dyn subfamily of GTP-binding proteins comprises a highly conserved NH_2-terminal GTPase domain, a plekstrin homology domain, a GTPase effector domain and a COOH-terminal PRD and displays relatively high homology with dyn1 [25]. Both, dyn1 and dyn2 are thought to function by GTP-triggered self-assembly into a helical collar around the neck of invaginated pits or caveolae followed by coordinated GTP hydrolysis and release of vesicles from PM [9, 26, 27].

In the current study we sought to define the role of the SH3A domain in ITSN-1s during caveolae endocytosis, with a focus on dyn2 oligomerization and enzymatic activity. Protein overexpression studies and specific assays for caveolae internalization applied on cultured human lung microvascular ECs, complemented by *in vitro* evaluation of dyn2 oligomerization and GTPase activity indicate that the SH3A domain of ITSN-1 has the unique ability to directly regulate dyn2 assembly–disassembly properties and GTPase activity at the endocytic site.

Materials and methods

Materials

Lung Human Microvascular ECs were from Cambrex (Walkersville, MD, USA); X-OMAT Blue XB-1 film from NEN Life Science Products (Boston, MA, USA); full-length rat dyn2 was kindly provided by Dr. Mark McNiven (Mayo Clinic, Rochester, MN, USA). cDNA FuGENE 6 Transfection Reagent from Roche Molecular Biochemicals (Indianapolis, IN, USA); Prolong Antifade kit, EnzCheck Phosphate Assay kit, NeutrAvidin-Texas Red and Alexa 488-conjugated antimouse IgG from Molecular Probes (Eugene, OR, USA), MicroBCA (bicinchoninic acid) Protein Assay Reagent Kit and SuperSignal Chemiluminescent Substrate (ECL) from Pierce (Rockford, IL, USA); EZ-Link Sulfo NHS-SS-Biotin and EZ-Link Sulfo NHS-Biotin from Fischer Scientific (Hanover Park, IL, USA); Blasticidin S HCl from Invitrogen (Carlsbad, CA, USA) and Glutathione Sepharose 4 Fast Flow from Amersham Biosciences (Pittsburgh, PA, USA).

All EM grade reagents were from EM Science (Forth Washington, PA, USA). All other reagents were from Sigma (St. Louis, MO, USA) if not otherwise specified. Relevant antibodies (Abs) were obtained from the following sources: anti-dyn mAb from Transduction Laboratories (Lexington, KY, USA), anti-dyn pAb from Cell Signaling Technology (Beverly, MA, USA), anti-dinitrophenyl (DNP) Ab from Bethyl Labs (Montgomery, TX, USA). Horseradish peroxidase (HRP)-conjugated anti-mouse IgG and HRP-conjugated anti-rabbit IgG from Cappel, Organon Teknika (Durham, NC, USA), anti-myc mAb was prepared as described [8].

ECs culture

Control and transfected lung human microvascular ECs were grown in medium 199-supplemented with 20% foetal calf serum as previously described [10].

Protein extraction

Cell lysates were prepared at 4°C in 20 mM 4-(2-hydroxyethyl)-1-piperazineethanesulfonic acid (HEPES)/KOH, pH 7.4, 2% Triton X-100, 100 mM KCl, 2 mM dithiothreitol (DTT), 2 mM ethylenediaminetetraacetic acid (EDTA) and protease inhibitor cocktail (Sigma). The ensuing lysates were clarified by centrifugation in a Beckman Optima Max-XP ultracentrifuge with a TLA-55 rotor, for 60 min. at 40,000 rpm (Beckman Instruments, Fullerton, CA, USA). Protein concentration was determined by the microBCA method with bovine serum albumin (BSA) standard.

ITSN-1s-SH3A, ITSN-1s-SH3E constructs and transfection procedure

Full-length human ITSN-1 cDNA (gift from Suzana de la Luna [Center for Genomic Regulation, UPF, and Centro de Investigacion Biomedica en Red de Enfermedades Raras [CIBERER-ISCIII], Barcelona, Spain), was used as a template to generate C-terminal myc-his tagged SH3A (residues 740–806) and SH3E domains (residues 1155–1214, based on cDNA sequence from GenBank Accession #AF114488). Primer pair **ITSN1L-SH3A-F-EcoRI**: 5′-AGTAGAATTCGCCACC**ATG**GCA GTAAAAGTGGTGTATTACCG-3′; **ITSN1L-SH3A-R-XbaI:** 5′-ACTTATCTAGATTCTGG GATTTTCTCTGCATAGTTTGC-3′

was used to generate the ITSN-1s SH3A domain that lacks the stop codon. The PCR cycling conditions were as follows: initial denaturation 94°C – 3 min., 25 cycles of denaturation, annealing and extension: 94°C – 30 sec., 58°C – 30 sec., 72°C – 1 min., followed by final extension 72°C – 7 min. and hold at 4°C. The resulting PCR fragment was digested with restriction enzymes *EcoR I* and *Xba I* (Invitrogen, underlined in primers) and subcloned into the *EcoR I–Xba I* restriction sites of vector pcDNA6/myc-His A (Invitrogen), resulting in construct pcDNA6A-ITSN1L-SH3A. A similar approach was used for myc-his-SH3E, using the following primer pair **ITSN1L-SH3E-F-EcoRI**: 5′-AGTAGAATTCGCCACC**ATGGCA**GCGGCAGTGTGCCAGGTGA-3′; **ITSN1L-SH3E-R-XbaI:** 5′-ACTTATCTAGAGTCTGTGGTCAGCTTCACAT-3′. The sequence of the pcDNA6A-ITSN-1-SH3A and SH3E was verified by DNA sequencing. All transfections were performed with FuGENE 6 transfection reagent, according to the manufacturer's instructions.

Expression of GST-SH3 domains in *Escherichia coli* and purification from bacterial lysates

ITSN-1s SH3 glutathione S-transferase (GST)-tagged domains were generated by subcloning into the pGEX-4T-1 vector (GE Healthcare Bio-Sciences Corp, Piscataway, NJ, USA) the PCR-amplified fragment corresponding to the ITSN-1L SH3A (residues 740–806), SH3D (residues 1074–1138), SH3E (residues 1155–1214) and SH3A-E (residues 740–1214) domains. The selection of the SH3 domains of ITSN-1s to be used in this study was based on the following criteria: the SH3A domain binds dyn2 with the highest affinity; the SH3E binds dyn2 and it was selected with the intent to demonstrate the specificity of the SH3A effects; SH3D is an SH3 domain of ITSN-1s that does not bind dyn2, while the entire SH3A-E complement was used to address if there is a cumulative effect between the SH3 domains of ITSN-1s in regulation of dyn2 oligomerization and GTPase activity. The primer pairs used to generate the domain fragments were as follows: for SH3A (**SH3A-F-EcoRI**: 5′-AGAATTCGTCGACGTAAAAGTGGTGTATTAC-3′; **SH3A-R-NotI**: 5′-AAGCGGCCGCTTATTATTCTGGGATTTTCC-3′). For SH3D: (**SH3D-F-EcoRI**: 5′-GAATTCAAAAA ACCTGAAATTGCC-3′; **SH3D-R-XhoI**: 5′-ATACCGCTCGAGTTATTAAGGGCTTAGAAG CTTTACATA). For SH3E: (**SH3E-F-EcoRI**: 5′-GAATTCCGCGGCAGTGTGCCAGGTG ATTGG-3′; **SH3E-R-NotI**: 5′-AAGCGGCCGCTTATTAGTCTGTGGTCAGCTTCAC-3′). For SH3A-E: (**SH3-F-EcoRI** 5′-AGAATTCGTCGACGTAAAAGTGGTGTATTAC-3′; **SH3E-R-NotI**: 5′-AAGCGGCCGCTTATTAGTCTGTGGTCAGCTTCAC-3′). The resulting PCR fragment was digested with *EcoR I* and *Not I* (Invitrogen) (as underlined in the primers) and subcloned into the *EcoR I–Not I* sites of PGEX-4T-1 vector. After the resulting cDNA vectors were verified by DNA sequencing to ensure sequence integrity, they were transformed into *E. coli* BL-21(DE3) pLysS (Invitrogen). The GST-fusion proteins were then purified by standard protocols from 1 mM isopropyl-β-D-thiogalactoside (IPTG)-induced bacteria. Maximum expression level was achieved 3 hrs after induction. Collected bacteria were resuspended in breaking buffer (100 mM HEPES/KOH, pH 7.0, 5 mM $MgCl_2$, 2 mM β-mercaptoethanol, 500 mM KCl and protease inhibitor cocktail for bacterial cells), incubated for 30 min. on ice with 1 mg/ml lysozyme, sonicated (3 × 30 sec., ½" disruptor, flat tip, horn, 70% amplitude). After addition of 1% Triton X-100 and incubation for 10 min. at 4°C, the bacterial lysates were clarified by centrifugation (45 min., 30,000 × *g*, 4°C), the supernatant was filtered through 45 μm Millex Syringe driven filters (Millipore, Billerica, MA, USA) and subjected to affinity chromatography on Glutathione Sepharose 4B column, according to the manufacturer's instructions. The concentration of GST-fusion proteins was determined with Pierce 660 nm protein assay reagent, and a BSA standard curve, as per manufacturer's instructions.

GST-ITSN1s plasmids, protein expression and purification

The full-length human ITSN-1s cDNA fragment (3663 bp) was generated by PCR amplification from ITSN-l cDNA with high-fidelity PCR enzyme (New England Biolabs, Ipswich, MA, USA), using the following primer pair: **ITSN1_F269-EcoRI**: 5′-AGTAGAATTC**ATG**GCTCAGTTTCCAACACCTT-3′ and **ITSN1_R3930-NotI**: 5′-CGTAGCGGCCGCTC**TCA**TTGCTGGCTTGGGTCCATG-3′. The PCR products of the full-length ITSN-1s were digested with restriction enzymes *EcoRI* and *Not I*, purified (Qiagen purification kit; Qiagen, Valencia, CA, USA), then cloned into pGEX-4T-1 vector at *EcoRI–Not I* sites and transformed into *E. coli* strain Top10 (Invitrogen). The plasmid DNA was extracted from several selected growing clones and the sequence of the full-length cDNA of ITSN-1s in frame inside the vector was confirmed. The plasmids DNA of selected clones were subsequently transformed into *E. coli* strain BL21(DE3)pLysS for protein expression. The expression of the GST-ITSN-1s fusion protein was induced with 0.1 mM IPTG and bacteria grown at 24°C for 14 hrs with shaking. The bacteria pellet was resuspended in breaking buffer, incubated for 30 min. on ice with 1 mg/ml of lysozyme, sonicated as above and clarified by centrifugation. The supernatant was then filtered through 45 μm Milex Syringe driven filters and the GST-ITSN-1s was purified as above; the purity was analysed by 10% SDS-PAGE gel electrophoresis followed by Coomassie Blue staining. The expression level of GST-ITSN-1s protein was high in several clones; the highly expressing clones were further selected depending on the ability of GST-ITSN-1s of binding dyn2. These specific clones were chosen for evaluation of full-length GST- ITSN-1s effects on dyn2 oligomerization and GTPase activity.

Biotin internalization and fluorescence microscopy

ECs, grown on plastic cover slips were subjected to internalization assay using biotin reagents, EZ-Link Sulfo NHS-SS-Biotin and EZ-Link Sulfo NHS-Biotin (Fischer Scientific) as in [10]. Cell monolayers were fixed and permeabilized with methanol, for 6 min., at –20°C, blocked with 1% BSA in PBS, pH 7.4, for 1 hr, RT. Internalized biotin was detected *via* neutrAvidin-Texas Red labelling for 1 hr, at RT. Transfected cells were selected *via* their blasticidin resistance as per manufacturer's instructions. Anti-myc mAb labelling in conjunction with antimouse IgG Alexa Fluor488 conjugated was used for detection of myc-SH3A expression. Images were obtained using identical acquisition parameters with a Zeiss Axio Imager M1 microscope equipped with ICc1 R3 colour camera (Zeiss, Thornwood, NY, USA).

Electron microscopy and morphometric analysis

Control and transfected cells grown on plastic Petri dishes were washed with PBS, fixed for 30 min., at RT with 1.5% glutaraldehyde in 0.1 M sodium cacodylate-hydrochloride buffer, pH 7.4 containing 5% sucrose, post-fixed in 1% OsO_4 in the same buffer, dehydrated in ethanol and finally embedded in Epon812 by standard procedures. Thin sections cut from Epon812 blocks were mounted on nickel grids, stained with uranyl acetate and lead citrate, and finally examined and micrographed in a Joel 1220 transmission EM. Morphometric analysis of abnormal caveolae profiles was performed as described previously [10]. Briefly, 15–20 sections per grid and three to five grids per block, from 8 Epon812 blocks, chosen at random from control and transfected ECs, were used. The morphological appearance was recorded on 50 micrographs (×30,000 standard magnification) for each experimental condition. The measurement of the

length PM on the electron micrograph used was performed as in [28]. The data were normalized per 100 μm length PM and are averages ± S.D. of three independent experiments.

Negative staining EM

Dyn2 structures were cross-linked with 0.5% final concentration of glutaraldehyde for 30 min., on ice, and then adsorbed onto formvar-coated nichel grids, recently exposed to glow discharge, fixed again with 1.5% glutaraldehyde in 0.2 mM sodium cacodylate buffer, pH 7.4, washed briefly through six drops of ddH_2O, negatively stained with 2% uranyl acetate, pH 4.5 and air dried.

SH3A-GST overlay

Immediately after electrotransfer, strips of nitrocellulose membranes, containing ECs lysates resolved on SDS-PAGE, were quenched for 1 hr, at RT, with 5% milk in 50 mM PBS, pH 7.5 and subsequently overlaid with 5 μg SH3A-GST in 20 mM Tris-HCl, 7.5, 3% BSA, 0.1% Tween-20 and 1 mM DTT, as in [29]. SH3A-GST interactions with endothelial proteins were detected *via* anti-GST pAb, followed by the appropriate reporter Ab and ECL detection.

Dyn2 sedimentation assay

Dyn2 assembly in oligomeric structures was performed in 200 μl buffer (40–150 mM NaCl, 20 mM HEPES pH 7.5, 1 mM EDTA, 4 mM DTT) with 0.5 μM dyn2, in the presence or absence of 100 μg/ml GST-SH3 domains or 250 μg/ml full-length GST- ITSN-1s, at RT for 10 min., as in [30]. Assembled and soluble dyn2 were separated by centrifugation at 60,000 × *g* for 15 min. in a TLA 100 rotor (Beckman Instruments), and analysed by SDS-PAGE and Coomassie Blue staining.

GTPase assay

The GTPase activity of dyn2 was measured by a continuous enzyme-coupled method for monitoring phosphate release, using the EnzChek® Phosphate Assay Kit (Molecular Probes) that provides an accurate measurement of the GTPase activity for several samples during the time course used in this study. Briefly, purified GST-dyn2 (0.5 μM) was incubated with or without GST-fusion proteins (1 μM) in the GTPase assay buffer (1 ml final volume reaction mixture). The reaction was initiated, after 10 min. of pre-incubation at 22°C, by addition of 500 μM GTP. The absorbance at 350 nm was recorded as a function of time for 30 min. Standard curves of low (0–10 nmol KH_2PO_4) and higher range (up to 50 nmol KH_2PO_4) were generated and used to determine the amounts of Pi released by dyn2-mediated GTP hydrolysis.

Results

Expression of the SH3A of ITSN-1 impairs caveolae internalization

Previous studies indicated that overexpression of full-length ITSN-1s or a construct lacking the SH3A domain inhibits caveolae endocytosis [10], and that the SH3A is a potent inhibitor of endocytosis [23]. Based on these observations, we sought to further study the function of the SH3A domain of ITSN-1 on dyn2 activity and caveolae trafficking. We used transient transfection of cultured ECs with myc-SH3A as in [10] and then we assessed the effects of this experimental manipulation on caveolae morphology and dynamics. First, control and myc-SH3A transfected cells were subjected to a biotin assay for caveolae internalization as in [10], followed by morphological and biochemical assessment of biotin uptake. Previous work demonstrated that this assay is a specific and reliable approach for addressing caveolae internalization in cultured ECs [10]. Studies using cholera toxin, a widely accepted marker for caveolae uptake [31, 32] or K^+ depletion to inhibit CME in cultured ECs subjected to biotin assay [10, 33] indicated the major contribution of caveolae to the internalization of biotinylated cell surface proteins. Caveolae-mediated uptake of biotinylated cell surface proteins is the dominant mechanism of internalization in ECs; the number of clathrin-coated vesicles in ECs is relatively small and their contribution to the internalization process is minor [1, 10, 34]. In control ECs subjected to biotin internalization, neutrAvidin-Texas Red staining revealed biotin association with vesicular structures spread throughout the cytoplasm, with perinuclear accumulation (Fig. 1A, a1, a1.1). In myc-SH3A transfected cells, the fluorescent staining and the accumulation of intracellular biotin were significantly reduced (Fig. 1A, a2). No staining or low-density of puncta were observed within intracellular space. The transfected cells were detected with anti-myc mAb [8], followed by antimouse IgG Alexa Fluor488-conjugated (Fig. 1A, a3). The fluorescent staining and accumulation of biotin in the perinuclear area were also reduced by reference to controls, when myc-SH3E, another SH3 domain of ITSN-1s that binds dyn2 was expressed in cultured ECs (not shown). Experiments using non-reducible biotin demonstrated the presence of biotin sequestered on the cell surface, with limited internalization (Fig. 1A, a4, a4.1). Biotin staining was occasionally detected in large puncta under the PM (Fig. 1A, a4.2, arrows). These findings suggested impairment in the ability of caveolae to internalize biotin. Quantitative evaluation of biotin uptake by ELISA applied on ECs selected based on their blasticidin resistance, demonstrated that the number of biotin molecules in all lysates prepared from transfected cells was markedly reduced (Fig. 1B). Biotin internalization was inhibited by 58.6% by reference to controls in SH3A transfected cells and by less than 30% in myc-SH3E transfected ECs, as calculated on three different points on the linear part of ELISA curve. The significantly lower inhibition caused by the SH3E on biotin internalization by comparison to the SH3A, suggests that despite binding dyn2 and presumably participating to its recruitment to the endocytic site, SH3E is not a major player in caveolae endocytosis (Fig. 1B).

Next, the ECs expressing the myc-SH3A were analysed at the ultrastructural level. Under control conditions caveolae exist as omega-shaped structures open to the extracellular environment through a short neck (Fig. 2A, a1 arrows, a2) or directly (Fig. 2A, inset a1.1), and as apparently detached spherical structures in the cytosol (Fig. 2A, a1 arrowheads) with an average diameter of ~70 nm [6]. Frequently, clusters of interconnected caveolae, in which the morphology of individual caveolae is evident, are observed

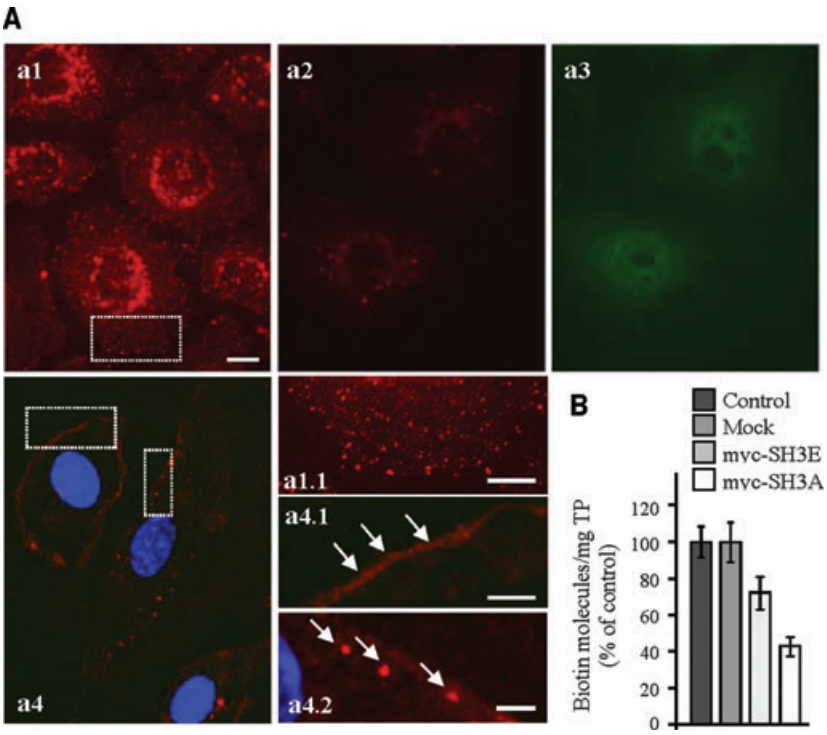

Fig. 1 Expression of the SH3A of ITSN-1 in cultured ECs impairs caveolae internalization. (**A**) In control cells subjected to biotinylation of cell surface proteins and internalization assay (37°C, 30 min.), neutrAvidin-Texas Red staining indicates a strong punctate pattern throughout the cytosol (a1, a1.1), with accumulation in the perinuclear area. ECs transiently transfected with myc-SH3A, selected based on their resistance to blasticidin, and then subjected to the internalization assay using cleavable biotin show limited neutrAvidin-Texas Red staining and some accumulation in the perinuclear area (a2). Anti-myc mAb followed by antimouse IgG Alexa Fluor488-conjugated was used to visualize transfected cells (a3). Use of non-cleavable biotin demonstrates sequestration of biotinylated proteins at the cell surface (a4, a4.1 arrows) and limited internalization. Within cells, biotin was often detected in large puncta under the PM (a4.2, arrows). Bars: 10 μm a1–a4; 5 μm – a1.1, a4.1; 3 μm – a4.2. (**B**) The number of biotin molecules present in ECs lysates prepared from controls, mock myc-SH3A and myc-SH3E transfected ECs was determined by ELISA in three to four different experiments. Ordinate: number of biotin molecules normalized per mg total protein (TP). Bars ± S.D.

(Fig. 2A, a3, a4). By contrast, in ECs transfected with myc-SH3A, we found significant alteration of caveolae morphology suggestive of an impaired membrane fission process (Fig. 2B). Frequently we observed caveolae with elongated necks (Fig. 2B, b1, and higher magnification b4–b6), and caveolae with their narrow necks surrounded by staining-dense collars (Fig. 2B, b7–b11). Large and uncharacteristic caveolae clusters (Fig. 2B, b1, arrow, b12–b14), anchored to the PM and open to the extracellular milieu or apparently without connection with the PM were observed in the intracellular space. Occasionally, some abnormal caveolae profiles are also detected under control conditions, but their frequency was significantly lower (Table 1). Morphometric analysis of these abnormal caveolae structures, in control and SH3A transfected cells, performed as in [10, 28], is summarized in Table 1. The diameter of the caveolar cavity, either as discrete vesicles or single caveolae attached to the PM was not detectably affected by myc-SH3A expression. Occasionally however, at the level of abnormal caveolae clusters we have recorded vesicular structures with bigger diameter (Fig. 2B, b12) or aberrant shape (Fig. 2B, b13, b14). Quantification of caveolae profiles, single or clustered, attached to and open to the apical PM indicated a 23.16% increase in SH3A-transfected cells by reference to controls, suggesting that the expression of the myc-SH3A may interfere with caveolae release from the PM and formation of discrete vesicular carriers. The presence of staining dense structures around invaginated vesicles and the narrowness of their necks strongly suggest that dyn2 recruitment occurred. Consistent with this idea, our previous studies using EM immunogold labelling of ECs overexpressing ITSN-1s, and thus, its SH3A domain, indicated increased association of dyn2 with elongated caveolae necks, many of them surrounded by staining dense collars [10].

Interestingly, similar findings involved clathrin-coated pits and vesicles. Clathrin-coated pits with elongated and constricted necks, Figure 2B, b1 (arrowhead), b2, b3, or clathrin-coated vesicles connected through narrow constriction, such as in Figure 2B, b3, were often recorded. Figure 2A, a5 shows for comparison, a segment from a control EC with two clathrin-coated pits open on opposite sides of PM. Based on these findings we concluded that expression of the SH3A may interfere with efficient recruitment and function of dyn2 at the endocytic site, resulting in impaired caveolae function during the transendothelial transport.

SH3A domain of ITSN-1s binds dyn2

Since to date biochemical studies of ITSN-1s/dyn interactions mediated by the SH3 domains have focused on dyn1 expressed predominantly in brain tissue, and since SH3 domains of ITSN-1s show differential binding activity to dyn1 and dyn2 [12, 35], here we sought to assess these interactions of ITSN-1s with dyn2, the ubiquitously expressed dyn isoform, in lung ECs. To this intent, GST pull-down experiments were performed with a subset of GST-tagged human ITSN-1 SH3 domains (SH3A, SH3D and SH3E), the GST-SH3A-E complement, as well as the full-length GST-tagged ITSN-1s. GST-SH3A is the most efficient in pulling down dyn2 from mouse lung lysates (Fig. 3A). GST-SH3E binds dyn2, but the

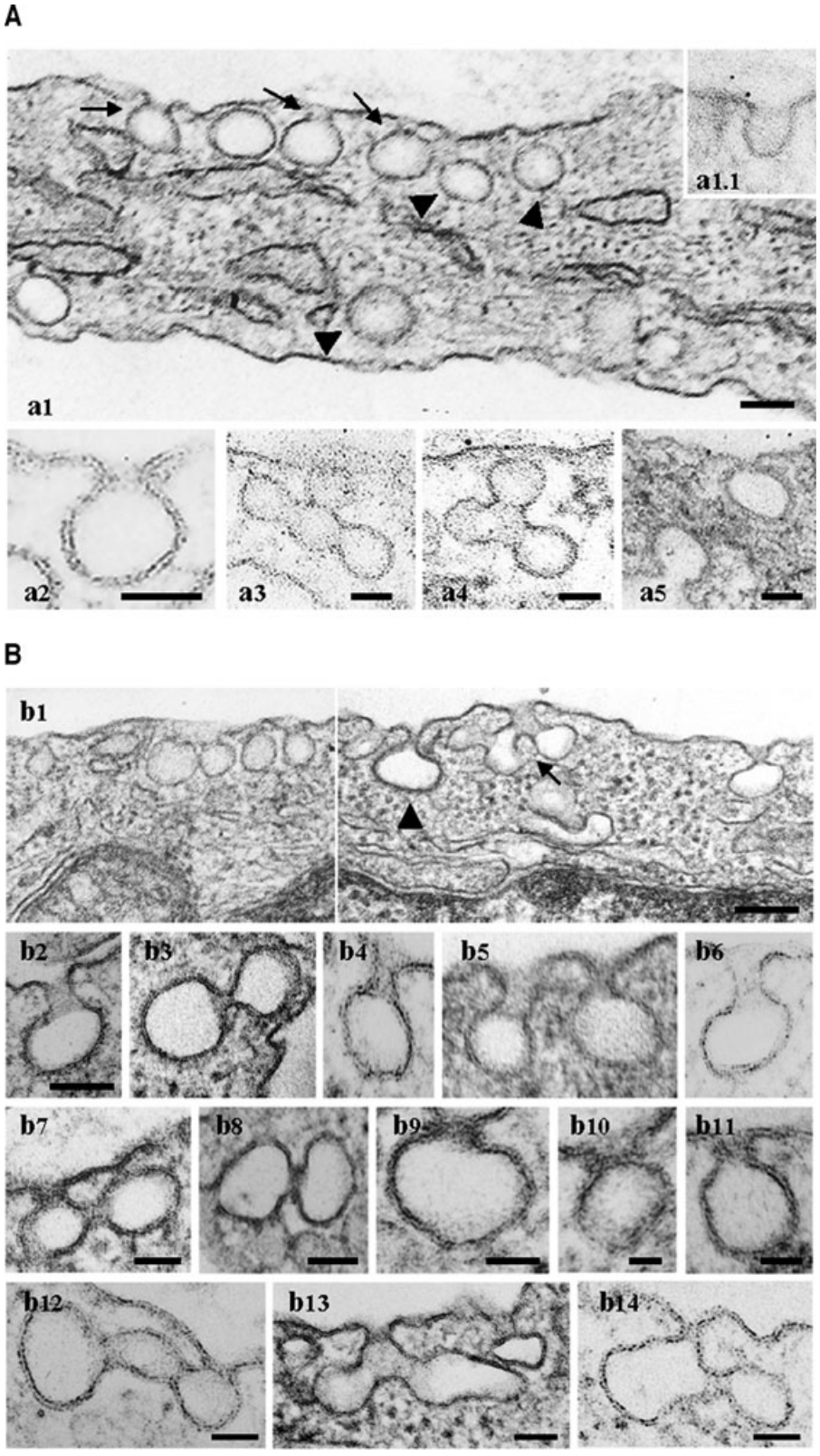

Fig. 2 Expression of the SH3A of ITSN-1 in cultured ECs causes abnormal caveolae morphology. (**A**) The electron micrographs show a segment of a control ECs with omega-shaped caveolae open to the extracellular environment through short necks (a1 arrows, a2) or directly (inset a1.1), and caveolae as apparently detached spherical structures in the cytosol (a1, arrowheads). Clusters of interconnected caveolae are shown in a3, a4. Two clathrin-coated pits open on opposite sides of the PM are shown in a5. Bars: 50 nm. (**B**) Electron micrographs showing highly magnified caveolar profiles with unusual morphology. Caveolae (b1, b4-b6) and clathrin-coated pits and vesicles (b1, arrowhead, b2) with elongated necks were frequently observed. The micrographs in panels (b7–b11) show staining-dense collars encircling the caveolae necks. Myc-SH3A expression causes unusual caveolae clustering (b1, arrow, b12–b14). Bars: 100 nm (b1); 70 nm (b2–b6); 50 nm (b7, b8, b12–14); 25 nm (b9–b11).

Table 1 Quantification of morphological changes caused by myc-SH3A expression in cultured ECs

Experimental condition	Abnormal caveolae clusters open to the apical side of EC	Apparently normal – omega-shaped caveolae	Single caveolae with staining dense rings around the neck	Caveolae with elongated necks
Control ECs	3 ± 0.4	82 ± 8	2 ± 0.3	8 ± 0.9
myc-SH3A transfected ECs	30 ± 5.3	15 ± 6.1	38 ± 4.2	34 ± 2.5

Fifty electron micrographs (30,000× magnification) per experimental condition, containing ECs profiles of control and myc-SH3A transfected ECs were used to count the number of (*i*) abnormal caveolae clusters open to the apical side of the endothelial PM, (*ii*) apparently normal caveolae, omega shaped, connected to the PM either directly or through short necks, (*iii*) caveolae with their neck surrounded by staining dense collars and (*iv*) caveolae with elongated necks (less than ½ of caveolar diameter). Quantification of these morphological characteristics and the measurement of the length PM on the electron micrograph used were performed as described previously [10, 28]. The data were normalized per 100 μm length PM and are averages ± S.D. of three independent experiments.

interaction is less efficient, while GST-SH3D does not bind dyn2. When the GST-SH3A-E or full-length GST-tagged ITSN-1s were used, dyn2 binding is efficient, but not augmented, suggesting that there are no cooperative effects among the SH3 modules in binding dyn2; alternatively, the possibility for improper folding, reported occasionally for other SH3 domains cannot be ruled out [36].

Gel electrophoresis analysis of GST-SH3 fusion proteins (Fig. 3B) by 5–20% SDS-PAGE shows the purity of GST-fusion proteins used in the study. Previous work using a range of GST-SH3 domains has shown that the GST tag does not interfere with binding affinity and characteristics of the SH3 domains towards dyn [30, 37]. Since the focus of this paper is on SH3A/dyn2 partnership, the GST-SH3A pull down studies were next complemented by a GST-SH3A overlay to address the specificity of the interaction and whether additional molecules are required for ITSN-1s interaction with dyn2, *via* the SH3A domain. To this intent, EC lysates subjected to SDS-PAGE and electrotransfer to nitrocellulose membrane were overlaid with the GST-SH3A fusion protein. The bound GST-SH3A, detected *via* GST pAb, revealed several interacting proteins (Fig. 3, lane + SH3A). We have identified by Western blot the identity of several proteins known to bind ITSN-1s *via* the SH3A domain. The 100 kD protein band bound by the GST-SH3A was immunoreactive to dyn2 Ab (Transduction Laboratories), (Fig. 3C, lane dyn2), while two other bands were identified as mSos (M_r 180 kD), and N-WASP (M_r 55 kD) (data not shown). Altogether, our findings indicate that in lung ECs, similar to neurons, ITSN-1s binds dyn2 *via* a subset of its SH3 domains. Moreover, since the GST-SH3A pulls down dyn2 from ECs lysates and interacts with a 100 kD protein immunoreactive to dyn2 Ab, we conclude that ITSN-1s directly interacts with dyn2, *via* the SH3A.

ITSN-SH3A stimulates dyn2 oligomerization

Transfection of cultured ECs with the SH3A caused abnormal caveolae morphology, stabilized caveolae necks and dyn2 collars, facilitating thus their detection by EM. These findings suggested a bona fide role of ITSN-SH3A in regulation dyn2 function at the endocytic site. We sought to test this hypothesis *in vitro* by analysing whether the multimerization state of dyn2 is affected upon SH3A binding. It has been previously reported that dyn forms sedimentable rings and spirals under low-salt conditions, while under physiological ionic strength dyn forms just very few rings [38]. To assess possible stimulatory effects of SH3A on dyn2 oligomerization, GST-dyn2, affinity purified on glutathione-coupled Sepharose 4B beads from IPTG-induced *E. coli* lysates, as described in [39] was pre-assembled into multimers, in the absence or in the presence of GST-SH3A, under conditions of physiological ionic strength [30, 40, 41]. Since GST alone does not affect dyn2 oligomerization [42] and since our pilot studies indicated that GST-SH3A and SH3A have same effects on dyn2 oligomerization we used the GST-SH3 fusion proteins without cleaving off the GST. Negative staining EM shows that purified dyn2 alone (Fig. 3D, d1) forms a high number of rod-like structures, few characteristic rings (d1, arrow) or incomplete rings, while in the presence of the GST-SH3A, 1:2 molar ratio (Fig. 3D, d2), the number of dyn2 rings (d2, black arrows and boxed area) and spirals (white arrows) is significantly increased. Inset in d2 shows higher magnification of dyn2 spirals (d1, upper gallery) and rings (d1, lower gallery). Detailed examination of dyn2 structures assembled in the presence of the GST-SH3A shows high protein content and well-defined structures, most likely due to a better packed in configuration. Also, the diameter of rings with GST-SH3A (52.1 ± 2.3 nm) was slightly smaller than that of the rings formed by dyn2 alone (58.8 ± 3.4 nm). Additional highly magnified, negatively stained dyn2 oligomeric structures, assembled in the absence (Fig. 3E, e1, e3, e5) or presence of the GST-SH3A (Fig. 3E, e2, e4, e6) are shown. Individual dyn2 rings (e1, e2) are similar to dyn1 rings. Like its neuronal isoform, dyn2 forms stacks of helical, interconnected rings (Fig. 3E, e3–e6). Frequently, dyn2 stacks formed in the presence of the SH3A displayed more rings (e6).

To quantify the effects of the SH3A on dyn2 oligomerization, purified GST-dyn2 was pre-assembled into oligomers, in 50 mM NaCl containing buffer, and a sedimentation assay was used to separate the assembled dyn2 from soluble dyn2, by centrifugation at 60,000 × *g*. The pellet (P) and supernatant (S) were analysed

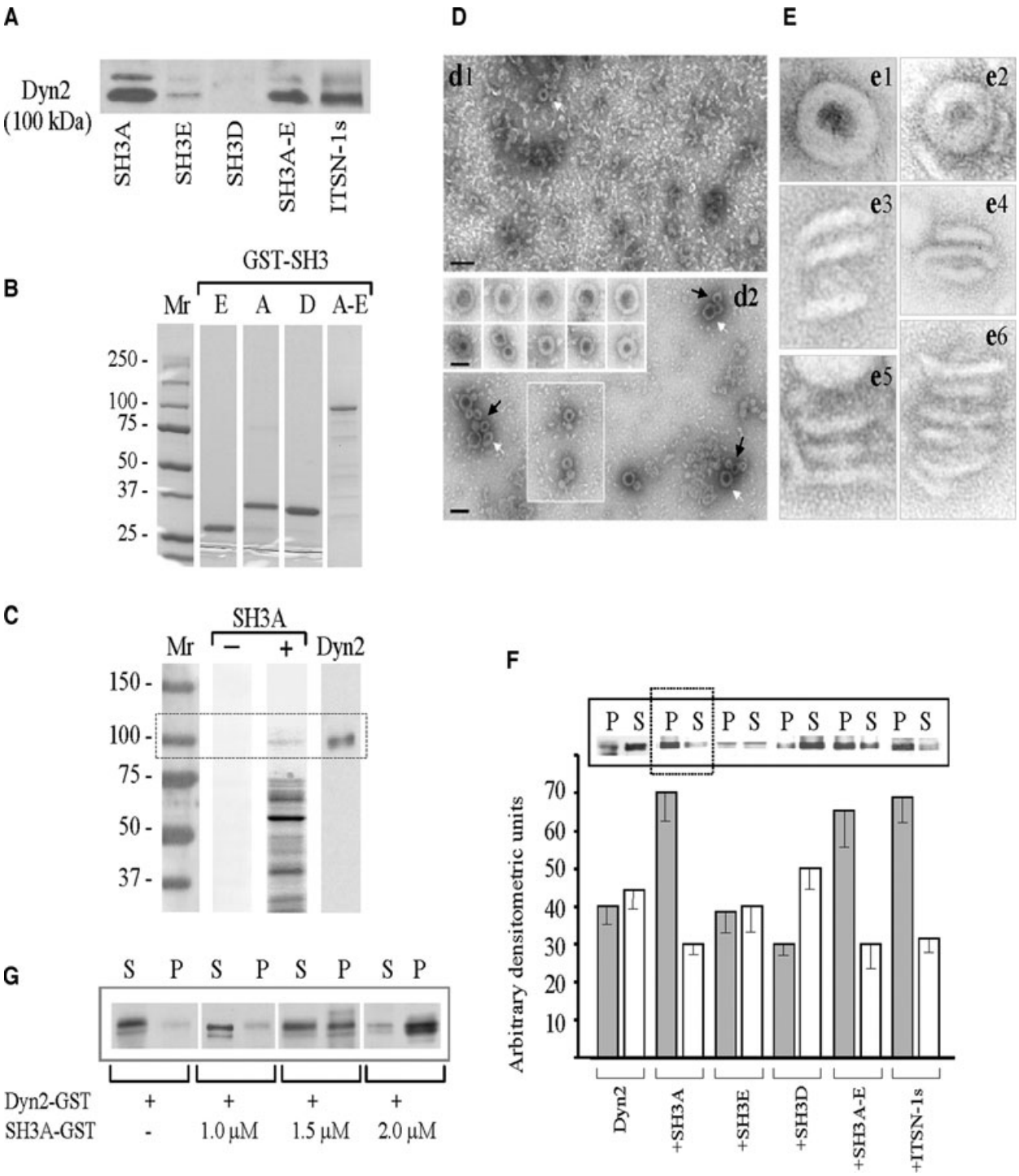

Fig. 3 SH3A stimulates dyn2 oligomerization. (**A**) SH3 pull-down assays were performed with mouse lung lysates (250 μg total protein) and GST-fusion proteins (~30 μg) encoding the SH3A, E and D, the SH3A-E complement as well as full-length ITSN-1s, coupled to Glutathione Sepharose beads. The proteins bound to the beads were eluted with SDS-PAGE sample buffer, subjected to electrophoresis and electrotransfer to NC membranes. The membranes were probed with anti dyn pAb. (**B**) Coomassie staining of a 5–20% SDS-PAGE shows the purity of the GST-SH3 fusion proteins obtained by affinity chromatography on Glutathione Sepharose 4B columns from 1 mM IPTG-induced *E. coli* lysates. Mr: molecular weight markers. (**C**) GST-SH3A overlay using nitrocellulose membranes containing the ECs proteins (100 μg), resolved by SDS-PAGE were incubated with the 5 μg GST-SH3A

(lane SH3A +); nitrocellulose membranes containing ECs proteins from the same experiment were reacted with anti-dyn Ab (lane Dyn2). A direct interaction between dyn2 and ITSN-1s *via* the SH3A domain is detected. (**D**) EM^{-} staining showing that purified dyn2 alone (d1), forms high number of rod-like structures and few characteristic rings (d1, white arrow), under physiological conditions (150 mM NaCl). Representative images show increase in the number of dyn2 rings (d2 and boxed area), and a significant increase in the number of dyn2 spirals (d2, arrows) when GST-SH3A is added. Galleries in the inset show high magnification of dyn2 spirals (upper gallery) and dyn2 rings (lower gallery). Bars: 100 nm (d1, d2); 50 nm (gallery insets in d2). (**E**) Highly magnified, negatively stained dyn2 structures assembled in the absence (e1, e3, e5) and in the presence (e2, e4, e6) of the GST-SH3A. All images are shown at the same magnification. (**F**) Affinity purified GST-dyn2 (0.1 mg/ml) was assembled into multimers, in the absence or in the presence of GST-SH3 fusion proteins using a low-ionic strength buffer. Oligomeric structures were separated from soluble dyn2 by centrifugation; the pellet (P) and supernatant (S) were analysed by SDS-PAGE followed by Coomassie Blue staining and densitometry. Under control conditions, dyn2 was found in both P and S fractions, slightly more in the S fraction. When GST-SH3A or GST-tagged full-length ITSN-1s are present, the equilibrium is shifted towards the oligomeric state (P fraction). The histogram represents the average amounts of dyn2 in the P and S factions in four different experiments. Densitometric analysis was performed with ImageJ 1.42l, Image Processing Software. (**G**) 2 μM GST-dyn2 was incubated for 10 min. at RT with increasing amounts of GST-SH3A at physiological salt (150 mM NaCl) concentrations. Samples were subjected to ultracentrifugation and the pellet (P) and supernatant (S) fractions were analysed by SDS-PAGE and Coomassie Blue staining.

by 5–20% SDS-PAGE, and Coomassie Blue staining. Under control conditions, GST-dyn2 is present in both P and S fractions (Fig. 3F), as previously reported for dyn1 [30]. When GST-SH3A was present, the amount of dyn2 in the soluble fraction diminishes, most of it being pelletable, consistent with a stimulatory effect of ITSN-SH3A on dyn2 oligomers formation. Densitometric analysis indicates that under these conditions the amount of dyn2 found in the P fraction is increased by more than 70%, compared to controls (Fig. 3F, histogram). SH3E, another SH3 domain of ITSN-1 that binds dyn2, does not affect dyn2 oligomerization. However, when the whole GST-SH3A-E complement or full-length GST-ITSN-1s were used, dyn2 oligomerization pattern is similar to the one obtained when the GST-SH3A is present, with more than 60% increase in the total dyn2 found in pellet (P), by reference to control conditions (Fig. 3F, histogram). Together these results suggest that the SH3A stimulates dyn2 assembly. It appears that SH3A may be the only SH3 domain of ITSN-1 able to modulate dyn2 oligomerization. When 2 μM dyn2 was incubated with GST-SH3A, under physiological buffer conditions, at different molar ratios (Fig. 3G) and then dyn2 oligomerization was analysed as above, we noticed increased GST-dyn2 oligomerization with increasing dyn2:SH3A ratio. A maximum stimulation of dyn2 oligomerization was detected when a molar ratio 1:1 for dyn2:SH3A reaction mixture was used.

ITSN-SH3A stimulates the GTPase activity of dyn2

To better understand the mechanisms through which ITSN-1s stabilizes dyn2 collars around the caveolae necks, we next examined the effects of the SH3A on dyn2 enzymatic activity. Evidence indicates that the GTPase activity of dyn and the efficient GTP hydrolysis in concert with a dyn conformational change are essential for endocytic vesicle fission from the PM [43]. Thus, we first measured the basal GTPase activity of dyn2 in the presence or absence of GST-SH3A, using a continuous enzyme coupled method for monitoring phosphate release. As shown in Figure 4A, The GST-SH3A stimulated the GTPase activity of dyn2 by reference to controls. To address the specificity of SH3A effects on dyn2 catalytic activity, next we used two other SH3 domains of ITSN-1. Neither GST-SH3E that binds dyn2, nor GST-SH3D that does not bind dyn2 stimulated the GTPase activity of dyn2. Similar observation was made when the full GST-SH3A-E was evaluated. This is somehow intriguing based on previous studies showing that the GTPase activity of dyn2 can be stimulated by dyn2 assembly in oligomeric structures [44] and our observation regarding the stimulatory effects of the GST-SH3A-E on dyn2 assembly (Fig. 3F). An inhibitory effect of the GST-SH3D on dyn2 GTPase activity (Fig. 4A) or particular folding properties when GST-SH3A-E is not part of the full ITSN-1s molecule, may explain this result. When the effect of full-length ITSN-1s GST-tagged was evaluated, the GTPase activity of dyn2 showed close values to those observed with SH3A (Fig. 4A), consistent with a stimulatory role of ITSN-1s, *via* the SH3A domain on dyn2 GTPase activity. However, the slightly lower efficiency in stimulation of dyn2 GTPase activity relative to SH3A alone, suggests a role for other elements of the ITSN-1s molecule in controlling the SH3A. The specificity of the stimulatory effects of the SH3A on dyn2 oligomerization and GTPase activity are also supported by several experiments in which the affinity purified GST-dyn2 preparations used contained a degradation product of about 85–90 kD, documented to be a truncated dyn lacking the PRD [42, 45]. Under these experimental conditions, the extent of increase in dyn2 oligomerization or GTPase activity in the presence of the SH3A were lower by comparison with the results obtained with non-proteolysed dyn2, indicating that in the absence of the PRD and thus, without SH3A binding, the extent of dyn2 oligomerization and GTPase activity are lower. To assay the effects of the SH3A on assembly-stimulated GTPase activity of dyn2, affinity purified dyn2 was diluted in a low-ionic strength buffer, conditions known to favour the formation of sedimentable dyn structures (Fig. 4B). The GTPase assays, for dyn2 alone and in the presence of GST-SH3A were started by addition of 500 μM GTP. The kinetics of GTP hydrolysis were analysed as above, for 30 min. time course. While the plots obtained for the GTPase activity of dyn2 alone show a sharp increase, a plateau and decrease after 18 min., the plot of the GTPase activity of dyn2 in the presence of the GST-SH3A follows a similar pattern only for the first 15 min. of GTP hydrolysis; after 15 min. the enzymatic activity is still high. This observation suggests that after 30 min. of GTP hydrolysis, dyn2–dyn2 interac-

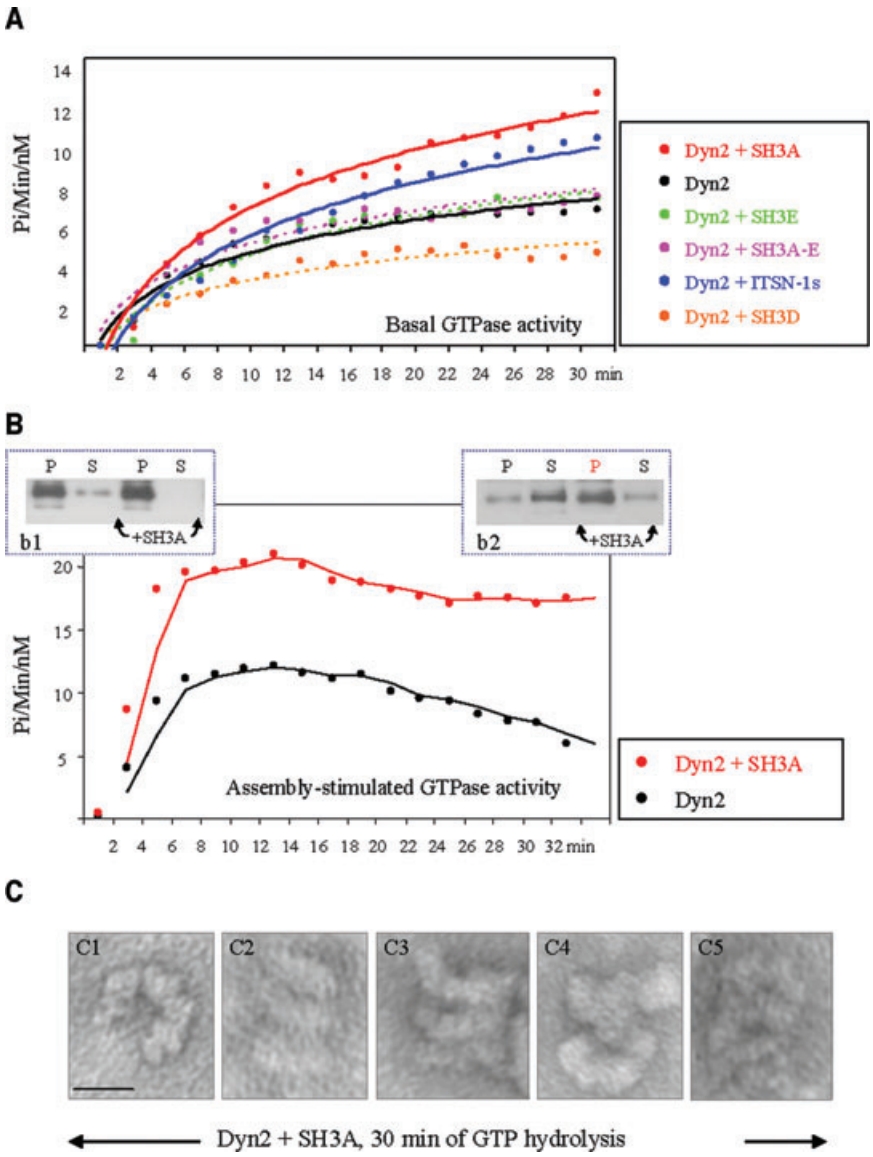

Fig. 4 GST-SH3A stimulates the GTPase activity of dyn2 and stabilizes dyn2 oligomeric structures. (**A**) The basal GTPase activity of dyn2 measured in the presence of different GST-SH3 domains of ITSN-1s as well as full length GST-tagged ITSN-1s. (**B**) Oligomeric dyn2 structures (b1, P fractions) were subjected to GTPase assay in the absence or presence of the GST-SH3A of ITSN-1. The GTPase activity of assembled dyn2 in the presence of GST-SH3A is higher by comparison to dyn2 alone. The GTPase activity of dyn2 decreases as GTP is hydrolysed and the dyn2 rings disassemble. In the presence of GST-SH3A, despite GTP hydrolysis, the GTPase activity of dyn2 remains high and apparently dyn2 conformation does not change. As shown, after 30 min. of GTP hydrolysis, the amount of pelletable dyn2 is significantly high (b2). (**C**) EM^{-} staining of stabilized dyn2 oligomeric structures, 30 min. after GTP hydrolysis. Dyn2 oligomeric structures – open rings (c1), stacks of rings (c2–c5), are stabilized, apparently unable to change their conformation. Bar: 50 nm.

tions persist and these still-assembled dyn2 structures account for the high GTPase activity. To confirm this assumption, parallel experiments were performed and the soluble (S) and sedimentable dyn2 fractions (P) were analysed by SDS-PAGE, electrotransfer and immunoblotting with anti-dyn2 Ab (Fig. 4B, b1, b2). Under control conditions (no GST-SH3A), after 30 min. of continuous GTP hydrolysis, dyn2 oligomeric structures disassembled as the GTPase activity of dyn2 decreases, while in the presence of the GST-SH3A the content of oligomeric structures is still high and the GTPase activity of dyn2 remains elevated (Fig. 4, b1 *versus* b2). EM^{-} staining (Fig. 4C) confirmed that when SH3A is present, dyn2 self-assembly is preserved; numerous dyn2 rings and stacks are detected. The high magnification of these structures shows open dyn2 rings (a) and frequently three to five dyn2 rings, as part of helical stacks. We believe these observations are consistent with the idea that despite high GTPase activity, dyn2/dyn2 interactions are preserved and dyn2 oligomeric structures are stabilized.

Discussion

In this study we have attempted to explain the functional significance of SH3A-mediated ITSN-1s/dyn2 interaction and to elucidate the means by which this interaction affects the overall function of dyn2 during endocytosis. Several SH3 domains have been shown to interact with the basic PRD of dyn1 or dyn2 and act as effectors of the GTPase activity [36, 37]. While most studies on this interaction

relate to the neuronal dyn1, recent studies demonstrated that the interaction of the PRD of the ubiquitously expressed dyn2 with SH3 domain containing proteins is required for dyn2-dependent caveolae and CME in non-neuronal cells [9, 46, 47]. Dyn2, similar to dyn1, forms rings when diluted in low-salt conditions, tubulates liposomes, it has a greater propensity for self-assembly than neuronal dyn1 and higher basal rates of GTP-hydrolysis [48, 49]. These characteristics may reflect dyn2 fine-tuning for constitutive endocytic and transcytotic processes that occur in ECs and other non-neuronal cells [50]. Evidence indicates that the SH3 domains inhibit endocytosis by interfering with dyn targeting to the endocytic site [47, 51], regulation of receptor function [42], stimulation of GTPase activity of dyn [37, 44], controlling dyn ring assembly or modulation of its disassembly [30, 52]. Limited evidence suggested that the SH3A domain of ITSN-1 may be unique in its ability to inhibit the endocytic process [23]. However, the specific way by which SH3A domain of ITSN-1s integrates in the overall function of dyn to cause inhibition of the endocytic activity and the molecular basis of SH3A uniqueness are not yet understood.

The studies described here reveal new and interesting characteristics of the SH3A domain of ITSN-1. First, the SH3A stimulates the oligomerization properties of dyn2. Second, in the presence of the SH3A the enzymatic activity of dyn2 increases, leading to increased GTP hydrolysis. Third, SH3A stabilizes dyn2 oligomeric structures, and as a result dyn2 rings are unable to change conformation, event thought to be required for dyn2 disassembly, recycling and vesicle release from the PM [43, 53]. The SH3A-stabilized dyn2–dyn2 interactions cause a prolonged lifetime for dyn2 collars and thus, impairment in free-transport vesicles formation and endocytosis. Significantly, the *in vitro* studies demonstrate that the SH3A effects on dyn2 oligomerization and GTPase activity are similar to those caused by full-length ITSN-1s, consistent with a fundamental contribution of the SH3A domain to the endocytic function of ITSN-1s. Altogether, the results add new functions for ITSN-1s during endocytosis: besides scaffolding the endocytic machinery, ITSN-1s modulates in a distinctive manner dyn2 self-assembly, disassembly and GTPase activity at the endocytic site.

Previous work and this study indicate that ITSN-1 is a major dyn2 binding partner [10, 54]. Immunogold labelling EM demonstrated that ITSN-1 preferentially associate with the necks of caveolae in all stages of the caveolar cycle, from fully to very narrow openings [6, 10]. Thus, ITSN-1s has the ability to recruit and bring together dyn2 molecules to the caveolae endocytic sites to generate the high dyn concentration needed for dyn self-assembly, increased enzymatic activity and subsequent, GTP hydrolysis. Disruption of SH3A mediated ITSN-1s/dyn2 interaction by transient transfection of cells with myc-SH3A caused abnormal caveolae morphology, distorted caveolae clusters and accumulation of caveolae with staining-dense collars around their necks, and as result, deficient caveolae internalization. The most likely explanation of these findings is the non-productive recruitment of dyn2 to the neck region of caveolae and impaired dyn2 function during caveolae release from the PM. In the context of *in vivo* studies, myc-SH3A expression, by disturbing the interaction between endogenous ITSN-1s and dyn2, interfered with the recruitment of dyn2 to the caveolae neck region. Yet, since ITSN-1s has two additional SH3 domains (SH3C and SH3E) capable of binding dyn2, and since there are up to five putative SH3 domain-binding sites within the PRD of dyn [34] the recruitment of dyn to the endocytic site is still possible. Not only dyn2, but also dyn2 bound to myc-SH3A can reach the endocytic site *via* SH3C and SH3E interactions. As our results indicate, dyn2 in the presence of the SH3A has higher ability to form oligomeric structures and increased GTPase activity. SH3A stimulates both basal and assembly-stimulated GTPase activity of dyn2. In the presence of SH3A at the endocytic site, dyn2–dyn2 interactions are stabilized and despite continuous GTP hydrolysis, dyn2 oligomers cannot disassemble. It appears that, SH3A holds up caveolae release from the PM and formation of free-transport vesicles, by prolonging the lifetime of assembled dyn2. The prolonged lifetime of assembled dyn2 led to impaired membrane fission and inhibition of caveolae endocytic function. The caveolar neck, the structure involved in establishing the short-lived connections of caveolae with the PM, shows here several structural modulations, many of them significant for caveolae fission from the PM. The caveolar cavity, however, maintains its shape and dimensions due to the stabilizing scaffold of caveolin-1 [6]. Interestingly, the abnormal caveolae clusters detected in the SH3A-transfected ECs, show caveolae connected by abnormal necks and occasionally vesicular structures with abnormal shape and size. Due to their caveolin-1 coat it is believed that caveolae maintain their dimensions and shape during their interactions with PM and trafficking [6, 8]. Detection in caveolin-1 null mouse of plasmalemmal vesicles, devoid of caveolin-1 raises the possibility that these caveolin-1 and clathrin-free structures may account for the vesicles with abnormal morphology detected within clusters. In addition, the recently reported interaction of ITSN with arfaptin2 [55], as well as studies of protein–protein interactions using the Ingenuity Pathways Analysis software [56], suggest that ITSN-1 may play a central role in influencing the function of BAR proteins. Arfaptin2 is a BAR domain containing protein with an elongated, crescent-shaped dimer of three-helix coiled-coils [57, 58] which can interact with membranes to induce membrane curvature or deformation [59]. Therefore, it is tempting to speculate that the interactions of ITSN-1 with dyn2 and arfaptin2 may possibly regulate membrane bending and caveolae formation, and thus, it may add new dimensions to ITSN endocytic function.

Previous studies indicated that other endocytic proteins and dyn1 partners, amphiphysin [30, 40, 60] and sorting nexin 9 [61] display similar properties. However, the SH3A of ITSN-1s seems to display an additional and rather distinct property in this regard. Dyn2 assembled into oligomeric structures in the presence of the SH3A is unable to change its conformation, disassemble and recycle for another round of membrane fission. Overexpressed SH3A could additionally sequester critical binding partners, still to be identified, in non-functional protein complexes and thus, their possible contribution to the impaired membrane fission, cannot be ruled out. Failure of either dyn2, assembled into collars around the caveolae necks, or other component of caveolae fission machinery to recruit downstream effectors should be considered, as well.

Altogether, our results suggest that ITSN-1s is not only required for dyn2 recruitment to the endocytic site, but also, through its SH3A domain, ITSN-1s is a key regulator of dyn2 assembly–disassembly and GTPase activity during caveolae and CME.

Acknowledgements

We are grateful to Dr. Suzana de la Luna (Center for Genomic Regulation, UPF, and Centro de Investigacion Biomedica en Red de Enfermedades Raras, Barcelona, Spain) for providing ITSN-1 cDNA and to Dr. Mark McNiven (Mayo Clinic) for his kind gift of full-length rat dyn2 cDNA. We thank Nicki Watson (Whitehead Institute, Cambridge, MA, USA) for technical support for EM studies. This work was supported by National Institute of Health Grants R01HL089462–01 and ARRA Suppl. (to S.P.), P01HL60678 (to A.M.), American Heart Association SDG0635175N (to S.P.) and start-up funds from Rush University Medical Center (to S.P.).

Conflict of interest

There is no conflict of interest to be disclosed.

References

1. **Palade GE, Simionescu M, Simionescu N.** Structural aspects of the permeability of the microvascular endothelium. *Acta Physiol Scand Suppl.* 1979; 463: 11–32.
2. **Predescu SA, Predescu DN, Palade GE.** Plasmalemmal vesicles function as transcytotic carriers for small proteins in the continuous endothelium. *Am J Physiol.* 1997; 272: H937–49.
3. **Mostov KE, Kraehenbuhl JP, Blobel G.** Receptor-mediated transcellular transport of immunoglobulin: synthesis of secretory component as multiple and larger transmembrane forms. *Proc Natl Acad Sci USA.* 1980; 77: 7257–61.
4. **Nesbitt SA, Horton MA.** Trafficking of matrix collagens through bone-resorbing osteoclasts. *Science.* 1997; 276: 266–9.
5. **Hemar A, Olivo JC, Williamson E, *et al.*** Dendroaxonal transcytosis of transferrin in cultured hippocampal and sympathetic neurons. *J Neurosci.* 1997; 17: 9026–34.
6. **Predescu SA, Predescu DN, Malik AB.** Molecular determinants of endothelial transcytosis and their role in endothelial permeability. *Am J Physiol Lung Cell Mol Physiol.* 2007b; 293: L823–42.
7. **Palade GE, Bruns RR.** Structural modulations of plasmalemmal vesicles. *J Cell Biol.* 1968; 37: 633–49.
8. **Predescu SA, Predescu DN, Palade GE.** Endothelial transcytotic machinery involves supramolecular protein-lipid complexes. *Mol Biol Cell.* 2001; 12: 1019–33.
9. **Oh P, McIntosh DP, Schnitzer JE.** Dynamin at the neck of caveolae mediates their budding to form transport vesicles by GTP-driven fission from the plasma membrane of endothelium. *J Cell Biol.* 1998; 141: 101–14.
10. **Predescu SA, Predescu DN, Timblin BK, *et al.*** Intersectin regulates fission and internalization of caveolae in endothelial cells. *Mol Biol Cell.* 2003; 14: 4997–5010.
11. **Yamabhai M, Hoffman NG, Hardison NL, *et al.*** Intersectin, a novel adaptor protein with two Eps15 homology and five Src homology 3 domains. *J Biol Chem.* 1998; 273: 31401–7.
12. **Okamoto M, Schoch S, Sudhof TC.** EHSH1/intersectin, a protein that contains EH and SH3 domains and binds to dynamin and SNAP-25. A protein connection between exocytosis and endocytosis? *J Biol Chem.* 1999; 274: 18446–54.
13. **Hussain NK, Yamabhai M, Ramjaun AR, *et al.*** Splice variants of intersectin are components of the endocytic machinery in neurons and nonneuronal cells. *J Biol Chem.* 1999; 274: 15671–7.
14. **Pucharcos C, Estivill X, de la Luna S.** Intersectin 2, a new multimodular protein involved in clathrin-mediated endocytosis. *FEBS Lett.* 2000; 478: 43–51.
15. **Adams A, Thorn JM, Yamabhai M, *et al.*** Intersectin, an adaptor protein involved in clathrin-mediated endocytosis, activates mitogenic signaling pathways. *J Biol Chem.* 2000; 275: 27414–20.
16. **Predescu SA, Predescu DN, Knezevic I, *et al.*** Intersectin-1s regulates the mitochondrial apoptotic pathway in endothelial cells. *J Biol Chem.* 2007a; 282: 17166–78.
17. **Das M, Scappini E, Martin NP, *et al.*** Regulation of neuron survival through an intersectin-phosphoinositide 3′-kinase C2beta-AKT pathway. *Mol Cell Biol.* 2007; 27: 7906–17.
18. **Sengar AS, Wang W, Bishay J, *et al.*** The EH and SH3 domain Ese proteins regulate endocytosis by linking to dynamin and Eps15. *EMBO J.* 1999; 18: 1159–71.
19. **O'Bryan JP, Mohney RP, Oldham CE.** Mitogenesis and endocytosis: what's at the INTERSECTIoN? *Oncogene.* 2001; 20: 6300–8.
20. **Tong XK, Hussain NK, de Heuvel E, *et al.*** The endocytic protein intersectin is a major binding partner for the Ras exchange factor mSos1 in rat brain. *EMBO J.* 2000; 19: 1263–71.
21. **Hussain NK, Jenna S, Glogauer M, *et al.*** Endocytic protein intersectin-l regulates actin assembly *via* Cdc42 and N-WASP. *Nat Cell Biol.* 2001; 3: 927–32.
22. **McGavin MK, Badour K, Hardy LA, *et al.*** The intersectin 2 adaptor links Wiskott Aldrich syndrome protein (WASp)-mediated actin polymerization to T cell antigen receptor endocytosis. *J Exp Med.* 2001; 194: 1777–87.
23. **Simpson F, Hussain NK, Qualmann B, *et al.*** SH3-domain-containing proteins function at distinct steps in clathrin-coated vesicle formation. *Nat Cell Biol.* 1999; 1: 119–24.
24. **Yu Y, Chu PY, Bowser DN, *et al.*** Mice deficient for the chromosome 21 ortholog Itsn1 exhibit vesicle-trafficking abnormalities. *Hum Mol Genet.* 2008; 17: 3281–90.
25. **McNiven MA.** Dynamin: a molecular motor with pinchase action. *Cell.* 1998; 94: 151–4.
26. **Takei K, McPherson PS, Schmid SL, *et al.*** Tubular membrane invaginations coated by dynamin rings are induced by GTP-gamma S in nerve terminals. *Nature.* 1995; 374: 186–90.
27. **Schmid SL, McNiven MA, De Camilli P.** Dynamin and its partners: a progress report. *Curr Opin Cell Biol.* 1998; 10: 504–12.
28. **Predescu D, Predescu S, Shimizu J, *et al.*** Constitutive eNOS-derived nitric oxide is a determinant of endothelial junctional integrity. *Am J Physiol Lung Cell Mol Physiol.* 2005; 289: L371–81.

29. **McPherson PS, Czernik AJ, Chilcote TJ, *et al.*** Interaction of Grb2 *via* its Src homology 3 domains with synaptic proteins including synapsin I. *Proc Natl Acad Sci USA.* 1994; 91: 6486–90.
30. **Owen DJ, Wigge P, Vallis Y, *et al.*** Crystal structure of the amphiphysin-2 SH3 domain and its role in the prevention of dynamin ring formation. *EMBO J.* 1998; 17: 5273–85.
31. **Schnitzer JE, Oh P, McIntosh DP.** Role of GTP hydrolysis in fission of caveolae directly from plasma membranes. *Science.* 1996; 274: 239–42.
32. **Tran D, Carpentier JL, Sawano F, *et al.*** Ligands internalized through coated or noncoated invaginations follow a common intracellular pathway. *Proc Natl Acad Sci USA.* 1987; 84: 7957–61.
33. **Larkin JM, Brown MS, Goldstein JL, *et al.*** Depletion of intracellular potassium arrests coated pit formation and receptor-mediated endocytosis in fibroblasts. *Cell.* 1983; 33: 273–85.
34. **Simionescu M, Simionescu N.** Endothelial transport of macromolecules: transcytosis and endocytosis. A look from cell biology. *Cell Biol Rev.* 1991; 25: 1–78.
35. **Solomaha E, Szeto FL, Yousef MA, *et al.*** Kinetics of Src homology 3 domain association with the proline-rich domain of dynamins: specificity, occlusion, and the effects of phosphorylation. *J Biol Chem.* 2005; 280: 23147–56.
36. **Herskovits JS, Shpetner HS, Burgess CC, *et al.*** Microtubules and Src homology 3 domains stimulate the dynamin GTPase *via* its C-terminal domain. *Proc Natl Acad Sci USA.* 1993; 90: 11468–72.
37. **Gout I, Dhand R, Hiles ID, *et al.*** The GTPase dynamin binds to and is activated by a subset of SH3 domains. *Cell.* 1993; 75: 25–36.
38. **Carr JF, Hinshaw JE.** Dynamin assembles into spirals under physiological salt conditions upon the addition of GDP and gamma-phosphate analogues. *J Biol Chem.* 1997; 272: 28030–5.
39. **Yao Q, Chen J, Cao H, *et al.*** Caveolin-1 interacts directly with dynamin-2. *J Mol Biol.* 2005; 348: 491–501.
40. **Takei K, Slepnev VI, Haucke V, *et al.*** Functional partnership between amphiphysin and dynamin in clathrin-mediated endocytosis. *Nat Cell Biol.* 1999; 1: 33–9.
41. **Tuma PL, Stachniak MC, Collins CA.** Activation of dynamin GTPase by acidic phospholipids and endogenous rat brain vesicles. *J Biol Chem.* 1993; 268: 17240–6.
42. **Scaife R, Venien-Bryan C, Margolis RL.** Dual function C-terminal domain of dynamin-1: modulation of self-assembly by interaction of the assembly site with SH3 domains. *Biochemistry.* 1998; 37: 17673–9.
43. **Marks B, Stowell MH, Vallis Y, *et al.*** GTPase activity of dynamin and resulting conformation change are essential for endocytosis. *Nature.* 2001; 410: 231–5.
44. **Yoshida Y, Takei K.** Stimulation of dynamin GTPase activity by amphiphysin. *Methods Enzymol.* 2005; 404: 528–37.
45. **Sever S, Muhlberg AB, Schmid SL.** Impairment of dynamin's GAP domain stimulates receptor-mediated endocytosis. *Nature.* 1999; 398: 481–6.
46. **Henley JR, Krueger EW, Oswald BJ, *et al.*** Dynamin-mediated internalization of caveolae. *J Cell Biol.* 1998; 141: 85–99.
47. **Szaszak M, Gaborik Z, Turu G, *et al.*** Role of the proline-rich domain of dynamin-2 and its interactions with Src homology 3 domains during endocytosis of the AT1 angiotensin receptor. *J Biol Chem.* 2002; 277: 21650–6.
48. **Warnock DE, Baba T, Schmid SL.** Ubiquitously expressed dynamin-II has a higher intrinsic GTPase activity and a greater propensity for self-assembly than neuronal dynamin-I. *Mol Biol Cell.* 1997; 8: 2553–62.
49. **Lin HC, Barylko B, Achiriloaie M, *et al.*** Phosphatidylinositol (4,5)-bisphosphate-dependent activation of dynamins I and II lacking the proline/arginine-rich domains. *J Biol Chem.* 1997; 272: 25999–6004.
50. **Liu YW, Surka MC, Schroeter T, *et al.*** Isoform and splice-variant specific functions of dynamin-2 revealed by analysis of conditional knock-out cells. *Mol Biol Cell.* 2008; 19: 5347–59.
51. **Barylko B, Binns DD, Albanesi JP.** Activation of dynamin GTPase activity by phosphoinositides and SH3 domain-containing proteins. *Methods Enzymol.* 2001; 329: 486–96.
52. **Yoshida Y, Kinuta M, Abe T, *et al.*** The stimulatory action of amphiphysin on dynamin function is dependent on lipid bilayer curvature. *EMBO J.* 2004; 23: 3483–91.
53. **Sweitzer SM, Hinshaw JE.** Dynamin undergoes a GTP-dependent conformational change causing vesiculation. *Cell.* 1998; 93: 1021–9.
54. **Elhamdani A, Azizi F, Solomaha E, *et al.*** Two mechanistically distinct forms of endocytosis in adrenal chromaffin cells: differential effects of SH3 domains and amphiphysin antagonism. *FEBS Lett.* 2006; 580: 3263–9.
55. **Scappini E, Koh TW, Martin NP, *et al.*** Intersectin enhances huntingtin aggregation and neurodegeneration through activation of c-Jun-NH2-terminal kinase. *Hum Mol Genet.* 2007; 16: 1862–71.
56. **Ahmed S, Bu W, Lee RT, *et al.*** F-BAR domain proteins: families and function. *Commun Integr Biol.* 2010; 3: 116–21.
57. **Peter BJ, Kent HM, Mills IG, *et al.*** BAR domains as sensors of membrane curvature: the amphiphysin BAR structure. *Science.* 2004; 303: 495–9.
58. **Tarricone C, Xiao B, Justin N, *et al.*** The structural basis of Arfaptin-mediated cross-talk between Rac and Arf signalling pathways. *Nature.* 2001; 411: 215–9.
59. **Itoh T, De Camilli P.** BAR, F-BAR (EFC) and ENTH/ANTH domains in the regulation of membrane-cytosol interfaces and membrane curvature. *Biochim Biophys Acta.* 2006; 1761: 897–912.
60. **Wigge P, Vallis Y, McMahon HT.** Inhibition of receptor-mediated endocytosis by the amphiphysin SH3 domain. *Curr Biol.* 1997; 7: 554–60.
61. **Soulet F, Yarar D, Leonard M, *et al.*** SNX9 regulates dynamin assembly and is required for efficient clathrin-mediated endocytosis. *Mol Biol Cell.* 2005; 16: 2058–67.